Design of an anthropomorphic PET phantom with elastic lungs and respiration modeling

David G. Black, Yas Oloumi Yazdi and Jeremy Wong
Department of Physics and Astronomy, University of British Columbia, Vancouver, BC, Canada

Roberto Fedrigo
Department of Physics and Astronomy, University of British Columbia, Vancouver, BC, Canada
BC Cancer Research Institute, Vancouver, BC, Canada

Carlos Uribe
Department of Functional Imaging, BC Cancer, Vancouver, BC, Canada
Department of Radiology, University of British Columbia, Vancouver, BC, Canada

Dan J. Kadrmas
Department of Radiology and Imaging Sciences, University of Utah, Salt Lake City, UT, USA

Arman Rahmim[a)]
Department of Physics and Astronomy, University of British Columbia, Vancouver, BC, Canada
BC Cancer Research Institute, Vancouver, BC, Canada
Department of Radiology, University of British Columbia, Vancouver, BC, Canada

Ivan S. Klyuzhin
BC Cancer Research Institute, Vancouver, BC, Canada
Department of Radiology, University of British Columbia, Vancouver, BC, Canada

(Received 27 December 2020; revised 6 May 2021; accepted for publication 10 May 2021; published xx xxxx xxxx)

Purpose: Respiratory motion during positron emission tomography (PET) scans can be a major detriment to image quality in oncological imaging. The impact of motion on lesion quantification and detectability can be assessed using phantoms with realistic anatomy representation and motion modeling. In this work, we develop an anthropomorphic phantom for PET imaging that combines anatomic fidelity and a realistic breathing mechanism with deformable lungs.
Methods: We start from a previously developed anatomically accurate but static phantom of a human torso, and add elastic lungs with a highly controllable actuation mechanism which replicates the physics of breathing. The space outside the lungs is filled with a radioactive water solution. To maintain anatomical accuracy and realistic gamma ray attenuation in the torso, all motion mechanisms and actuators are positioned outside of the phantom compartment. The actuation mechanism can produce custom respiratory waveforms with breathing rates up to 25 breaths per minute and tidal volumes up to 1200 mL.
Results: Several tests were performed to validate the performance of the phantom assembly, in which the phantom was filled with water and given respiratory waveforms to execute. All parts demonstrated expected performance. Force requirements were not exceeded and no leaks were detected, although continued use of the phantom is required to evaluate wear. The motion of the lungs was determined to be within a reasonable realistic range.
Conclusions: The full mechanical design is described in this paper, as well as a software application with graphical user interface which was developed to plan and visualize respiratory patterns. Both are available online as open source files. The developed phantom will facilitate future work in evaluating the impact of respiratory motion on lesion quantification and detectability in clinical practice.
 [https://doi.org/10.1002/mp.14998]

Key words: anthropomorphic phantom, motion correction, motion management, pet, phantoms - physical, quantitative imaging/analysis

1. INTRODUCTION

Positron emission tomography (PET) imaging is widely used in oncology for tumor detection, monitoring, and quantification. A leading factor that can adversely affect the quality of thoracic PET images is respiratory motion during the scans.[1] In normal respiration, the amplitude of diaphragm movement is on the order of 1.5–2 cm,[2] while deep inspiration may result in 7–13 cm diaphragm displacement.[3] For clinical PET scanners with spatial resolution around 0.4–0.5 cm full-width at half-maximum (FWHM), motion of this magnitude can lead to effective resolution closer to 1 cm.[4,5] This can reduce contrast for small lesions (e.g. cancer metastases[6]), worsen lesion detectability, and introduce bias in the measured standardized uptake values (SUVs). In some cases, the measured values of functional metrics such as mean and

maximum SUV (SUVmean, SUVmax) can directly affect therapy planning and post-treatment outcome analysis.[7,8] For larger lesions, respiratory motion may likewise introduce bias in radiomic features that quantify lesion shape and texture.[9–11] Additionally, the mismatch between PET and computed tomography (CT) images due to motion may lead to errors in attenuation correction and scatter estimation.[12,13]

Hence, there is an extensive ongoing effort to understand and evaluate the effect of respiratory motion in routine clinical PET imaging, particularly with respect to thoracic lesion detectability and quantification.[14–16] For a quantitative assessment of such effects, it is necessary to obtain the ground truth activity values of lesions without respiration. In human subjects, respiratory gating and/or breath hold techniques can be used to reduce the effects of respiratory motion to obtain *in vivo* proxy measures of ground truth lesion activities, but these techniques are imperfect, subject to increased noise, and may be challenging in practice.[17] In contrast, physical phantoms with various levels of complexity and realism offer a powerful experimental approach where the ground truth activity is precisely known. One of the most common approaches is to mount a rigid torso phantom on an actuated platform that can generate translational motion with a precisely known trajectory, such as the QUASAR system (Modus QA, Ontario, Canada). For example, such an approach was used by Liu et al.,[18] who reported underestimation of SUVmax by 28% for 1 cm lesions due to motion. In another study that used a similar approach, contrast recovery for hot spheres in a phantom was found to be reduced by nearly 50% due to motion.[19] With continuing advances in PET scanner sensitivity and resolution,[20] as well as development of novel image quantification paradigms,[21] it becomes of interest to evaluate the effects of respiratory motion under more anatomically realistic conditions. Rigidly moving thorax phantoms, no matter how geometrically realistic, do not simulate several important effects of respiratory motion, namely motion of organs and lesions with respect to the ribcage, or changes in attenuation due to lung volume change. In order to simulate such effects, relative movement of internal compartments inside the phantom must be implemented.

The goal of this work was to develop an anthropomorphic phantom for PET imaging, which combines anatomic fidelity and a realistic breathing mechanism with deformable lungs. We propose and test an approach wherein elastic lungs are manufactured from 3D-printed molds, and actuation is performed by means of creating a negative pressure differential inside the thorax – similar to how real breathing occurs in humans. We build upon an existing phantom previously developed by Kadrmas et al.,[22,23] henceforth referred to as "Probe-IQ" (Image Quality Probe), which has previously been static and not used to study motion effects. To the best of our knowledge, Probe-IQ to this day has the highest level of anatomical realism in the field. In the development of the motion-enabled phantom and lung actuation mechanism described in this paper, we use the shell and rib-cage of the original Probe-IQ phantom, but add custom-built elastic lungs with trachea, and an electronically controlled linear actuator to drive the lung deformation. The phantom is intended for use in PET imaging to evaluate the effect of respiratory motion on lesion quantification.

TABLE I. Comparison of existing anthropomorphic phantoms of interest.

Name	PET/CT/MRI	CM	RM	LM	SS	Lesions
Probe-IQ + Respiratory motion capabilities	✓/✓/×	×	✓	✓	✓	✓
Probe-IQ[22,23]	✓/✓/×	×	×	×	✓	✓
Wilhelm[24]	✓/✓/✓	✓	✓	✓	×	✓
Alderson[25]	✓/✓/×	✓	✓	×	✓	×

CM, cardiac motion; RM, respiratory motion; LM, liver motion; SS, skeletal structure.

Several other anthropomorphic phantoms with focus on respiratory motion modeling in PET/CT imaging have been developed in the past; they are listed in Table I in comparison to the motion-enabled Probe-IQ. While Wilhelm[24] has the most realistic overall motion of any existing device, it lacks any bone structure, which is important for accurately modeling the gamma ray attenuation and scatter. Conversely, Alderson[25] has bones as well as respiratory and cardiac motion; however, its anatomy is simplified and it does not support the addition of lesions. Besides PET/CT imaging, several anthropomorphic phantoms have been developed specifically for radiation dosimetry and radiotherapy planning.[26,27] In such phantoms lungs are typically inflated using a ventilator that applies positive air pressure.[28–30] However, driving lungs by ventilation is difficult when they are surrounded by an incompressible medium, for example, a radioactive water solution. In contrast, our approach is based on a more realistic principle of creating a negative pressure differential inside the thorax, forcing the lungs to inflate; the advantages of this approach are described later in the manuscript.

In this paper, we carefully consider the technical challenges associated with the proposed phantom design, and describe the functional requirements. To facilitate the re-use of our work by other groups, the implementation of the phantom is described in detail, including open-sourced schematics, materials, and software. Finally, we test the function of the completed phantom assembly and perform CT scans with artificial lung lesion tracking to validate the proposed method of lung actuation.

2. MATERIALS AND METHODS

2.A. Design overview

The Probe-IQ phantom enhanced with respiratory motion capabilities aims to achieve the following:

- Anatomical accuracy
  - Builds off the static anatomical accuracy of Probe-IQ and achieves realistic lung motion.
  - Avoids any unrealistic parts like connecting rods or metal components in the torso.

- All materials carefully selected with reference to mass attenuation coefficients[31] or tests[24] to resemble human tissue.

- Respiratory motion control

- Able to achieve a wide range of breathing rates and tidal volumes (i.e. air displaced between inhalation and exhalation). Namely, at least up to 25 breaths per minute at 1 L tidal volume; typical relaxed breathing is 500 mL tidal volume at 15–20 breaths per minute.[32]
- Has highly controllable, repeatable, consistent breathing motion to generate high quality data, but also can include occasional disrupted breaths or inconsistencies, as would happen in a real patient.
- Realistic actuation principle.

In addition, safety is a concern, as the phantom is filled with approximately 15 L of radioactive solution (300 to 1000 MBq of radioactivity per scan) for PET acquisitions. The design must avoid leaks, and minimize the possibility of large spills. Easy fill-ability of the phantom is also desirable to reduce radiation exposure to users and to increase usability.

The respiratory motion-enabled Probe-IQ phantom involves three main components: (a) elastic and realistically shaped lungs, (b) an actuation method, and (c) a control system (electronics and software). The overall structure can be seen in Fig. 1 and all design files and code can be accessed in the Open Source Section at the end of this paper. The lungs are located inside the rib cage of the existing Probe-IQ phantom (A), and surrounded by a radioactive water solution creating the nonspecific radioactivity background typically present in oncological PET images. The lungs are connected to the atmosphere by a breathing tube (trachea) (F), which can be sealed at the neck. The actuating mechanism is positioned below the phantom (B, C, D), where the pelvis of a human would be located. It is outside the field of view of the PET scanner with a standard axial extent, so as not to create image artifacts. The phantom operates by piston-actuated passive breathing, as explained below and seen in Fig. 2.

To achieve respiratory motion with the lungs, the mechanism modulates the volume or pressure of the whole phantom in a manner analogous to real human breathing. Since the phantom is sealed, rigid, and entirely filled with water, except for the air-filled lungs, changing its volume by ΔV induces an equal volume change of ΔV in the lungs. Instead of compressing the air in a sealed set of lungs, the pressure requirement of the actuating mechanism can be dramatically decreased by opening the lungs to the atmosphere once the phantom has been filled and sealed. Contrary with intuition, the lungs do not collapse under the pressure of the water since the water volume is constant and cannot expand to fill the vacant space created if the lungs were to collapse. In effect, a relative negative pressure is created in the liquid anterior to the lungs, just as human breathing relies on negative intrapleural pressure. Now, when the volume of the torso is changed, that volume of air is simply exhaled to or inhaled from the atmosphere (Fig. 2).

To prepare the phantom for imaging, the lungs, organs, and bones are positioned inside the thorax, and the lungs are pressurized using a Schrader valve (Fig. 3) before completely filling the phantom with radioactive water solution. A valve in the base plate, at the highest point in the torso, is used to release the displaced air (Fig. 3). Once the phantom is filled and sealed, the lungs are opened to the atmosphere.

With the phantom setup, the user can define custom respiratory patterns, rates, and volumes using a graphical user interface. The piston then moves along the defined trajectory for the duration of a scan, causing the lungs to expand and contract. The next three sections describe the lungs, breathing mechanism, and software in more detail.

2.B. Lungs

The lung shapes were derived from a CT scan of an adult male and simplified using mesh editing software (Blender Foundation, Amsterdam) to reduce the cardiac notch and

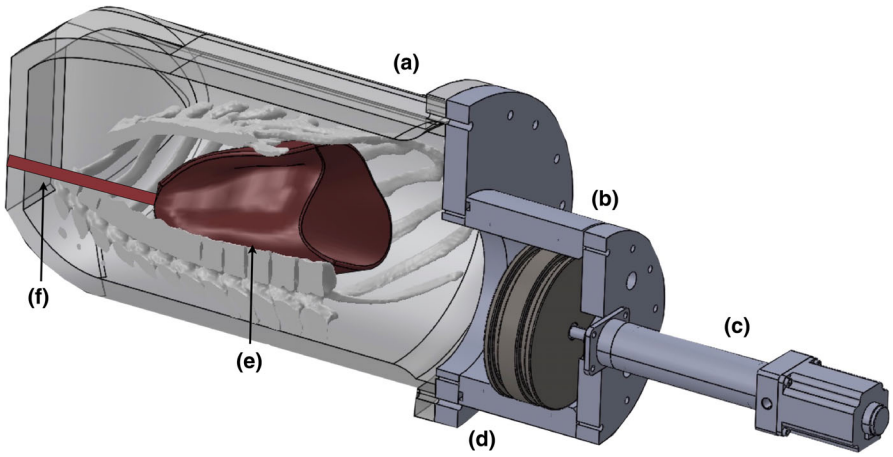

FIG. 1. Overview of phantom design. A: existing thorax shell and bone structure (liver and heart compartments included but not pictured). B: Piston and cylinder for torso volume modulation. C: linear actuator. D: custom-designed base-plate allows compatibility with existing Probe-IQ phantom. E: flexible lung inserts of silicone elastomer. F: breathing tubes (trachea) connect lungs to atmosphere to allow air transfer during inhalation and exhalation.

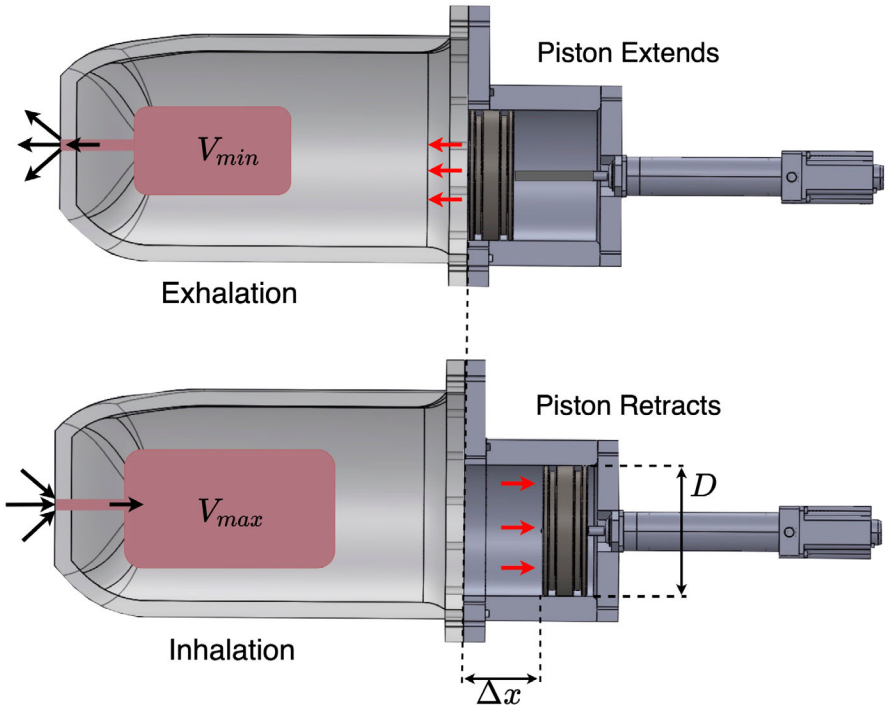

FIG. 2. Respiration modeling by modulating the volume of the phantom, mediated by incompressible fluid. Air flows into and out of the lungs through the trachea as the piston extends and retracts.

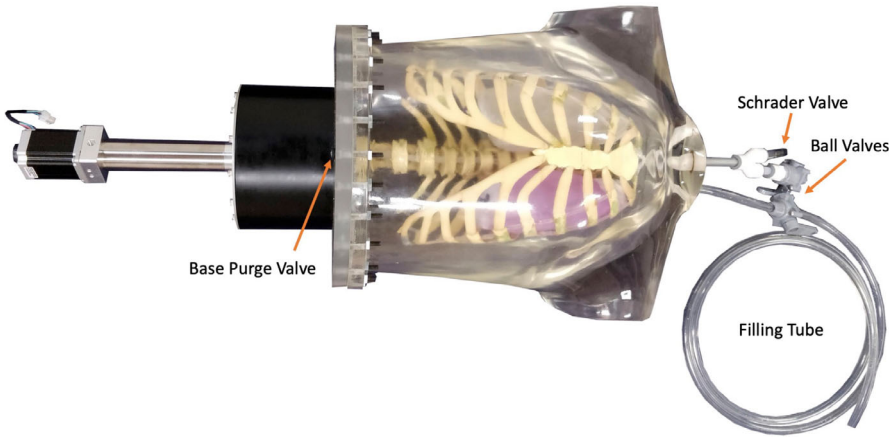

FIG. 3. Assembled phantom with filling system.

make the right and left lungs more symmetrical [Fig. 4(a)]. This was done primarily for ease of fabrication, but also to avoid unpredictable expansion and contraction of complex shapes which differ between the lungs. The lungs were designed to have a realistic adult size postexhalation, with a volume of 1650 ml each. This ensures that during normal breathing the lungs only expand, and do not compress or fold in an irregular manner. The dimensions of the lungs are approximately 18.0 cm (height) by 10.0 cm (width) by 12.7 cm (depth). The lungs have uniform wall thickness of 2 mm and can optionally be coupled directly to the piston using thin cables (not visible on reconstructed PET images) to force a specific longitudinal flex pattern.

A thru-wall fitting commonly used in prosthetics was custom manufactured using Delrin plastic [Fig. 4(b)]. This is attached medially near the top points of both lungs to connect air tubes which lead through a Y-connector to a single tube to the outside of the phantom, much like bronchi connecting to the trachea. One of three ports in the neck area of the phantom provides the inlet for the breathing tubes. The lungs are held in place in the superior/inferior axis using the trachea, and in the lateral and anterior/posterior axes using the rib cage. At the inlet of the trachea, near the neck of the phantom, another Y-connector splits the airway into a large ball valve and a Schrader valve which are used to alternatively pressurize and seal the lungs or allow free airflow (Fig. 3).

The lungs were manufactured by rolling Chlorosil-35 (Ottobock, Germany), a silicone-based elastomer, onto a dental plaster lung model which was cast inside a 3D-printed negative mold. Following high temperature vulcanization, the

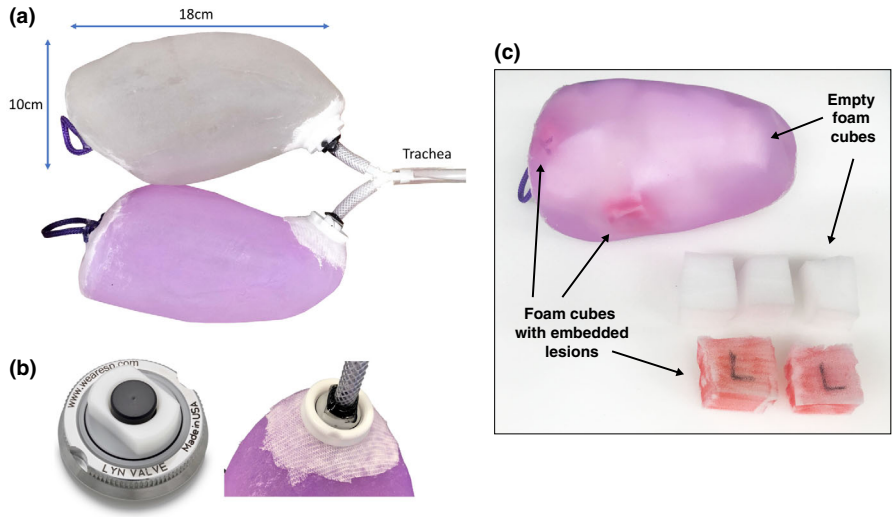

FIG. 4. (a) Lungs with bronchi and trachea. Bottom loops can be used to couple the lung motion directly to the piston if desired. Both lungs are the same material with different dyes. (b) Original (left) and custom manufactured plastic (right) thru-wall fitting (ESP LLC, New Jersey, USA) used to attach trachea to the lungs. The lung silicone is compressed between the twin flanges and creates an air-tight seal. (c) To hold artificial lesions in custom locations, the lungs were filled through the air opening with compressed foam cubes, some of which had lesions embedded (marked with red color).

FIG. 5. Left: Piston with dual O-rings; Center: Cylinder with O-ring to seal against base plate; Right: Piston in Cylinder. Threaded blind hole in piston to couple lung motion is visible.

silicone material is durable, long-lasting, and thermostable, yet flexible to allow contraction and expansion. The material was previously tested in another phantom.[10] A thin piece of stiffer plastic with a mounting point for a cable was placed in a silicone pocket at the base of each lung. To hold artificial lesions near the wall of the lungs, small silicone pockets can be added before vulcanization, or after, using silicone adhesive. A further method for holding lesions outside the lungs is to place them in slots cut into low-water/air resistance foam placed within the phantom compartments as previously described with the Probe-IQ phantom.[22,23]

To hold artificial lesions inside the lungs for our motion validation experiments, the lungs were filled with soft foam cubes (uncompressed size 3–4 cm). Upon lung expansion, the foam cubes expand to fill the empty space, while helping maintain a constant relative lesion location [Fig. 4(c)]. Each lung was filled with 78 grams of foam (Active Foam Products, Inc., series DF1200 super soft, firmness 10) and contained three spherical lesions made from an epoxy resin (diameter 5–7 mm). The lesions were inserted into foam cubes and positioned in three different locations in the right and left lung respectively.

2.C. Breathing mechanism

To modulate the volume, both a rubber "diaphragm" membrane stretched across the entire phantom base and a piston mechanism were considered. After preliminary testing, the diaphragm mechanism was found to be unreliable, so the piston mechanism was chosen. This consists of a large cylinder attached directly to the base plate of the phantom. A piston is driven back and forth in the cylinder using a linear actuator to create the

volume change. The actuator works against the piston friction, water viscosity and inertia, and elastic forces in the lungs.

The mechanism consists of three major components: the piston and cylinder (Fig. 5), the base and mounting plates, and the linear actuator. Each is described below, before outlining their cumulative capabilities. The assembled mechanism is shown in Fig. 7.

2.C.1. Piston and cylinder

To achieve and maintain the tight tolerances (e.g. ±0.1 mm over a 14 cm diameter) required to form a seal, while avoiding attenuation and scatter from metallic components, both the piston and cylinder were manufactured from Delrin acetal plastic. Delrin is dimensionally stable and machinable, has low water absorption, and a low friction coefficient of 0.2, which reduces the required actuator load.[33] The cylinder has 27 mm-thick walls to avoid warping, and a chamfer at the mouth of the cylinder ensures easy insertion of the piston without scratching the surfaces important for the seal.

Two opposing factors played a role in determining the inner diameter of the cylinder. The larger the diameter, the smaller the piston displacement must be for a given volume change, and thus the lower the speed requirement on the linear actuator. However, a larger piston is harder to machine within tolerance and to fit onto the base plate. A diameter of 14 cm was chosen as a compromise. At this diameter, the piston displacement for a given volume change is approximately equal to the axial lung extension for a given tidal volume in humans.[3] For example, a piston movement of 3 cm leads to a volume change of 500 ml, which is a typical relaxed adult tidal volume. According to Wade et al.,[3] the lungs should very roughly extend on average 1.5 cm for 500 ml tidal volume, though this varies widely between individuals. The system's stroke is 8 cm, so with the chosen dimensions, tidal volumes of up to 1232 ml are possible, which constitute realistic deep breaths.

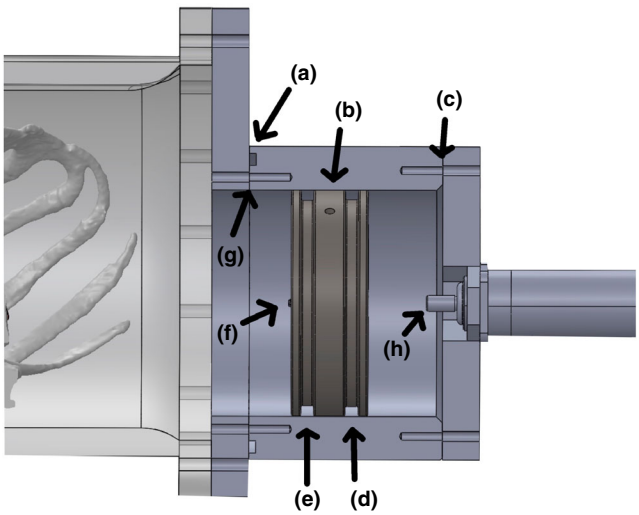

FIG. 6. Cross-section of the piston drive mechanism. A: Cylinder face O-ring groove. B: Inter-O-ring vent hole. C: Actuator mounting plate screw holes. D: Backup O-ring groove. E: Main O-ring groove. F: Insert for mounting piston-lung motion-coupling cable. G: Cylinder to base plate mounting screw holes. H: The linear actuator screws directly into the piston (see H in Fig), leaving minimal clearance between the piston and the actuator mounting plate to maximize the stroke length of the piston.

The piston has two O-ring grooves which ensure alignment inside the cylinder and provide a watertight dynamic seal (Fig. 6). The cylinder's inner surface was honed to 8–16 μ in RA roughness to minimize wear and friction, and to improve the seal. A size −429 Buna-N rubber O-ring was selected for the same reasons, as well as its radiation resistance and large contact area for effective sealing. The cylinder is screwed to the base plate with an O-ring, and the actuator mounting plate screws into the backside of the cylinder. The flanged actuator is mounted directly to this plate. In this way, misalignment is minimized, and the whole structure is modular and easy to assemble and disassemble. The linear actuator screws directly into the piston, leaving minimal clearance between piston and mounting plate to maximize the positional range of the piston. The opposite side of the piston has an attachment point into which a cable to the lungs can optionally be fastened, or a rod can be attached to move an internal diaphragm. This gives flexibility in mounting and motion options.

2.C.2. Mounting plates

Two plates were made to mount the respiration mechanism to the existing Probe-IQ phantom, and to attach the linear actuator to the cylinder assembly. The former was fabricated from polycarbonate to avoid backscatter that could be caused by metal. Its dimensions were extracted from a CT scan of the phantom. A large, central hole was included for the piston, as well as 36 holes for mounting the cylinder to the base plate and the base plate to the phantom base flange in a secure, sealed manner with the load distributed evenly. Finally, a sealable hole was drilled into the plate at the highest point of the torso cavity to purge air.

As the second plate is further away from the scanner's gantry and supported fully by the cylinder, it was fabricated from 3 mm-thick, waterjet-cut aluminum. The actuator mounts directly to the plate via a flange to minimize misalignment. This plate seals in any small leaks that potentially make it through the piston O-rings.

2.C.3. Linear actuator

The actuator type and model were selected based on the criteria outlined in Table II, as well as cost.

We set out to achieve a 1000 ml tidal volume at 25 breaths per minute. While the piston was designed to provide up to 1232 ml tidal volume, and the 90 mm actuator stroke supports the full range of piston motion, a linear speed of 54 mm/s is required to reach 25 breaths per minute at this amplitude (assuming the actuator accelerates instantly, which is reasonable since the chosen actuator has a maximum acceleration of 1667 mm/s^2). The required force is approximately the sum of the piston friction (F_f), the water inertia (F_i), and the elastic stretching of the lungs (F_e):

TABLE II. Linear actuator design requirements.

Criterion	Desired	Chosen actuator
Speed	54 mm/s	167 mm/s
Stroke	90 mm	90 mm
Force	900 N	890 N
Duty Cycle	100%	100%
Durability	High	5200-scan estimated life
Controllability	High	See in text
Weight	Low	≈1.5 kg

$$F = F_f + F_i + F_e \tag{1}$$

Using the Parker O-Ring Handbook, the friction is approximately $F_f = 250$ N. To calculate the inertial force, assume the actuator accelerates to the 54 mm/s velocity within 0.5 cm, which constitutes an acceleration of $a = 0.292$ m/s^2. As a very conservative estimate, suppose all 17.3 kg of water in the phantom accelerate at this rate. Then:

$$F_i = (17.3kg)\left(0.292m/s^2\right) = 5N \tag{2}$$

This is negligible compared to the frictional force. Similarly, the static pressure on the piston can be ignored because the water pressure on the front of the piston and the air pressure on the back cancel out.

To find the force required to stretch the lungs, assume that the lungs are cylindrical, and use the thin-wall approximation to find the hoop stress in one lung. This, however, also assumes that Hooke's Law holds for rubber-like elastomers. Merrit and Weinhaus[34] found that this is not the case, and that after an initial linear section, the required pressure to increase the radius sharply falls off. Thus, Hooke's Law provides an overestimate for large extensions. Let ℓ, r, t be the cylindrical lung's length, radius, and wall thickness, respectively, and $\ell_0 = 200$ mm, $r_0 = 52$ mm, and $t_0 = 2$ mm be the initial values. These give the expected initial volume of 1700 ml, as well as an initial material volume of $V_0^{mat} \approx 2\pi r_0 t_0(\ell_0 + r_0) = 21000$ mm^3. Rubber is incompressible, so $V_0^{mat} = V_f^{mat}$. Thus:

$$t \approx \frac{2100}{r(\ell + r)} \tag{3}$$

Now using hoop stress, $\sigma_H = \frac{r\Delta p}{t}$, and Hooke's Law, $\sigma_H = \frac{t_0 - t}{t_0}E$, we obtain an expression for the required force applied by the piston:

$$F_e = (0.14)^2 \frac{\pi}{4} \frac{2100}{r^2(\ell + r)} \left(1 - \frac{2100}{rt_0(\ell + r)}\right) E.$$

The elastic modulus, E, of silicone rubbers can be estimated roughly from the Shore A durometer using Ruess' Equation: $\log_{10} E = 0.0235S$ - 0.6403.[35] Since the lung silicone has Shore A hardness 35, $E \approx 1.5$ MPa. Thus, to achieve a 1000 ml volume increase and about 6.6 cm lung extension,[7] we take $\ell = 266$ mm and $r = 56.8$ mm. Then $F_e = 199$ N.

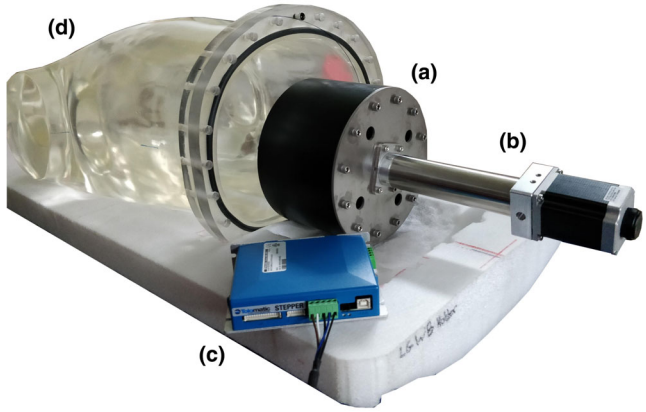

FIG. 7. Assembled breathing mechanism (A. cylinder containing piston, B. linear actuator, and C. stepper motor control box) with empty phantom (D).

Thus, according to Eq. (1), a conservative estimate for the maximum force required from the actuator is $F = 450$ N. Applying a factor of safety of 2, considering that these calculations were approximate, piston friction could increase with wear, and foam around the lungs could increase the pressure requirement, the linear actuator should be able to supply around 900 N of force.

To move the piston, a lead-screw actuation mechanism is preferred because of its superior controllability over pneumatic cylinders and other types of linear actuators. The phantom has to move continuously for the duration of the scan, which can be around 30 min, so the duty cycle has to be 100% for extended periods of time. A ball screw mechanism, which has much less friction than ACME lead screws, allows for continuous use and a long lifetime.

Based on these criteria, an ERD15 (Tolomatic, USA) ball-screw linear actuator was chosen, along with a stepper motor with encoder feedback. This relatively low-cost actuator is designed to run continuously and fulfills the load, stroke, and speed requirements. Assuming we carried out 30 min scans at the calculated force, at 25 breaths per minute and 1000 ml tidal volume, the actuator would have an estimated life of 5200 scans (according to manufacturer specifications[36]). The ERD's low profile and simplicity allow it to be mounted as seen in Fig. 7. The actuator position is accurate to within 0.03 mm per cm of movement.[23] Together with the 1.8 °/step stepper motor and 2000-count encoder feedback, this facilitates exact velocity and acceleration control.

The force analysis was verified during testing by running the actuator at 40% force, where it stalled, and then at 60%, where it ran smoothly. This implies that the required force is around 50% of the actuator's force capability, which, given the chosen safety factor of 2, means the required force corresponds closely to the derived value.

2.D. Software and electrical design

The Tolomatic ERD15 actuator is driven by a stepper motor with encoder feedback, which is controlled by stepper

driver hardware from Tolomatic. The goal in this control system is to create realistic, consistent, repeatable lung motion with flexibility in breathing rate and amplitude, as well as the ability to include breathing inconsistencies for added realism. Two distinct control methods were created for the phantom and are described below. The first is simple and fast to setup while the second provides more realism, so each is useful in different applications.

First, a free Windows application (described below) can be used to communicate with the stepper driver over USB to configure the actuator. The second option is analog position control. Here, a 0–10 V analog signal can be input to the driver, which moves to the corresponding position. Control through ethernet and Modbus RTU over RS-485 are also possible, but neither was investigated in this work.

2.D.1. USB interface

The actuator manufacturer provides a software interface called Tolomatic Motion Interface (TMI) to communicate with its stepper controllers over USB. While the software is primarily used to configure the driver initially, it can also be used to control the actuator's motion directly. Moves can be defined with a certain acceleration, deceleration, velocity, and goal position. These moves can then be combined in any order to form a repeating series of up to 16 moves. Taking the simplest example, one may define just 2 moves, one to 45 mm, and one to 1 mm, and cycle between these two positions indefinitely. By combining more positions, however, and altering their accelerations and decelerations, a wide variety of motion patterns can be achieved, including realistic respiratory cycles.

The problem with this method is that it is difficult to visualize what the respiratory cycle will look like based on a series of linear position, velocity, and acceleration values. A graphical user interface (GUI) was therefore developed in Python to allow motion planning and visualization of the lung volume as a function of time (Fig. 8).

In the application, the user can define the breathing rate, amplitude, and base lung volume. We used published models[24] to identify a physiologically representative equation for a respiratory curve [Eq. (4); x = amplitude, t = time], which can be scaled and shifted to match the desired, user-defined breathing parameters. This curve is plotted in green in Fig. 8.

$$x = e^{-1.71668t}\frac{0.0106 + 2.3313t + 0.535t^2 + 3.959t^3}{2.3062 + 0.3517t - 0.6487t^2 + 0.1177t^3} \quad (4)$$

The user can then define up to four moves with position, velocity, acceleration, and deceleration, and place them in any order. The corresponding motion profile is generated through iterative kinematic simulation of the actuator, and plotted in real time, in red in Fig. 8, as the parameters are changed. With the red actuator plot overlaid onto the green desired plot, the optimal set of motion parameters can be determined. It is also possible to save configurations in automatically formatted JSON files to be loaded later.

This control method is simple because the respiratory cycle is visualized, input into user-friendly software, and relayed to the actuator directly over USB. While a variety of motions can be achieved in this manner, it is nonetheless limited by the discrete nature of a set of individual moves. To overcome this problem, at the cost of simplicity, analog control can be used.

2.D.2. Analog position control

The second method controls the ERD15 actuator using a 0–10 V analog signal. The voltage range is mapped onto the positional range of the actuator so that a given voltage causes the actuator to move to that position. Thus, arbitrary continuous waveforms can be realized by the actuator, if they do not exceed the configured acceleration and velocity values. Figure 9 shows the setup used to generate the analog signal. The voltage was provided by an MCP4725 Digital to Analog Converter (DAC), controlled via the I2C GPIO pins of a Raspberry Pi microcomputer. The encoder feedback is read by the Raspberry Pi, and any control software is run on the Raspberry Pi.

For the actuator to respond to the analog input voltage, analog control must be enabled through a digital input. Thus, digital COM is tied to the power supply ground, and a voltage divider is used to provide the 24 V needed to enable motion. An N-channel MOSFET whose gate voltage is set by the Raspberry Pi switches the enable input between 0 and 24 V.

With this setup, arbitrary waveforms can be saved as CSV files on the Raspberry Pi. A Python program converts the volumetric data to actuator positional curves using the piston geometry, and then to voltages using the voltage-position mapping. The voltages are sent via I2C to the DAC, where they are converted to analog voltages and input into the actuator, thus generating the desired lung motion.

3. RESULTS: TESTING AND VALIDATION

To validate the efficacy of the proposed phantom design, testing of the complete assembly was performed. The primary criteria for evaluation were realism in the trajectory, symmetry between the lungs, consistency of movement, and controllability, as well as validation of the force requirements and mechanical integrity. Two sets of experiments were performed, with optical tracking of continuous lung motion and CT scans acquired with a "step-and-shoot" technique.

3.A. Optical tracking experiments

The phantom was setup in the single O-ring configuration and was filled with water. Filling was performed using the neck ports. The lungs maintained their position and shape when opened to the atmosphere, and the piston was then run back and forth continuously for 30 min with cameras mounted above and on either side of the phantom. No water leakage to the outside of the phantom was observed. The piston was first set to move at 30 mm/s and then 40 mm/s, both

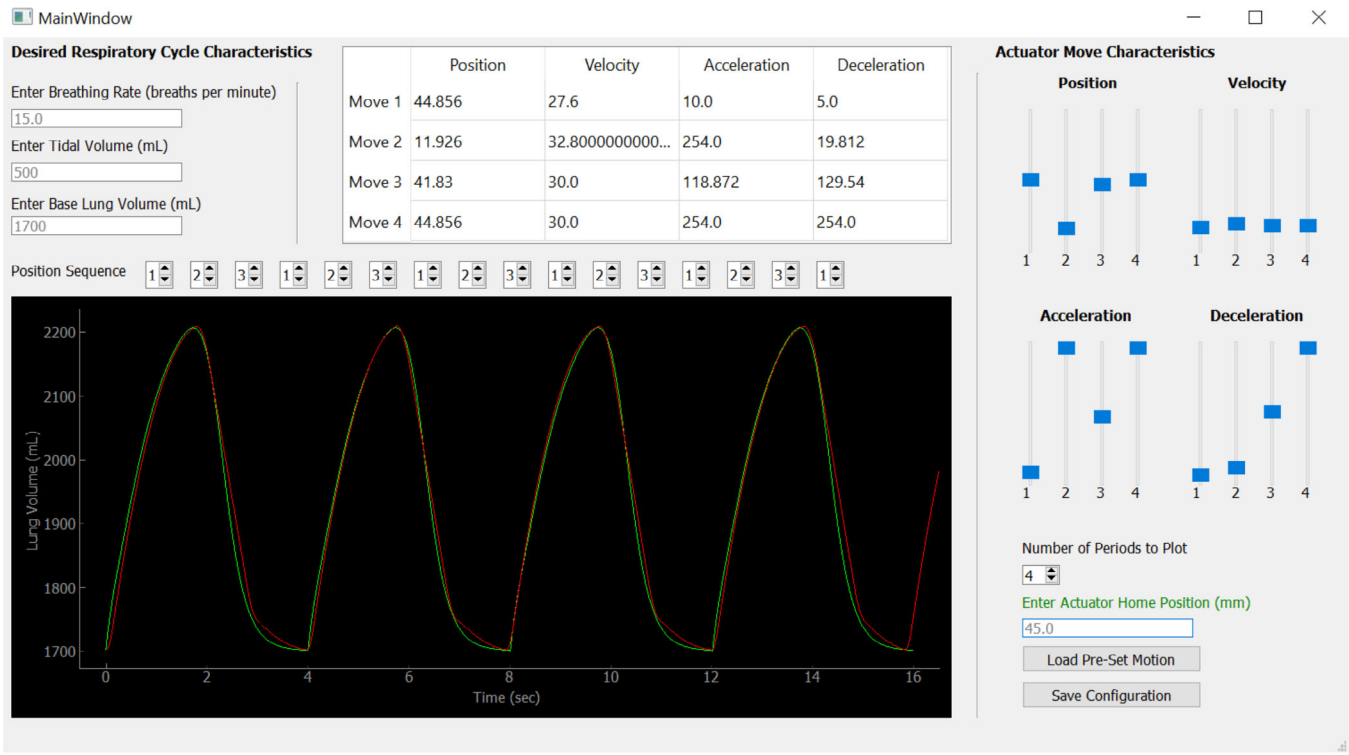

FIG. 8. Screenshot of motion planning application. The green curve is the desired respiratory cycle, while the red is the pattern carried out by the phantom based on the GUI inputs.

with a 58 mm amplitude. This corresponds to 892 ml tidal volume at 15 and 21 breaths per minute, respectively.

The resultant trajectory is shown in Fig. 10. The videos are available in the open source materials. Qualitatively, the breathing looked realistic, and included some rib motion and flexing, which adds to the realism. The lungs' maximum and minimum positions were ascertained from the videos at all angles. There is little difference between the right and left lung, as seen when viewed from above (Fig. 10, right image).

Analysis of the actual displacements allows comparison to the average trajectories previously determined for adult males. The results are given in Table III, in comparison with previously published values.[3] These results show that the lungs naturally expand slightly more in circumference and extend less axially than desired. However, they are within the reasonable realistic adult male range given by Wade's measurements and his observation of variability between individuals.

Finally, the consistency of the motion was analyzed by tracking three markers placed on the left lung for 20 breaths. The frames were binned using the known frame rate of the video and the set breathing rate such that only frames showing the lungs at 100%, 75%, 50%, 25%, and 0% inhalation were used. The motion of each point formed a scatter plot through which a line was fitted, and the root-mean-squared (RMS) error was calculated as an indicator of the motion's consistency. The resulting RMS errors were 0.74, 0.52, and 0.54 mm from the straight line. Note that the tracking error in the position measurements was about ± 1 mm, so the results show that the lung motion was consistent between the breaths.

After one test that included a total of 40 min of almost continuous motion, the phantom was emptied, and the drive mechanism was dismantled and inspected. There were no signs of wear in the mechanism, which would have indicated a problem. The O-ring remained very well lubricated, and the cylinder wall behind the O-ring was dry. It is expected that with continued good lubrication the chance of leakage will remain very low. Since the phantom rests on an absorbent sheet throughout operation and is left in isolation until the isotopes have decayed to background levels, individual drops that may get through the piston do not represent a concern, especially as they remain contained within the cylinder. However, the second O-ring can also be installed on the piston to further improve the seal.

3.B. CT scans of the phantom

To more precisely characterize the motion and deformation of foam-filled lungs with lesions, a series of seven CT scans corresponding to 0% to 100% inflation in equal intervals were carried out. Four images from the series are plotted in Fig. 11(top). At 0% inflation, a small amount of lung wall buckling can be seen, which can be resolved in future scans by increasing the internal lung air pressure during the phantom filling. Artificial lesion motion can be seen in the images, and the foam contributed to a more realistic texture inside the lungs,

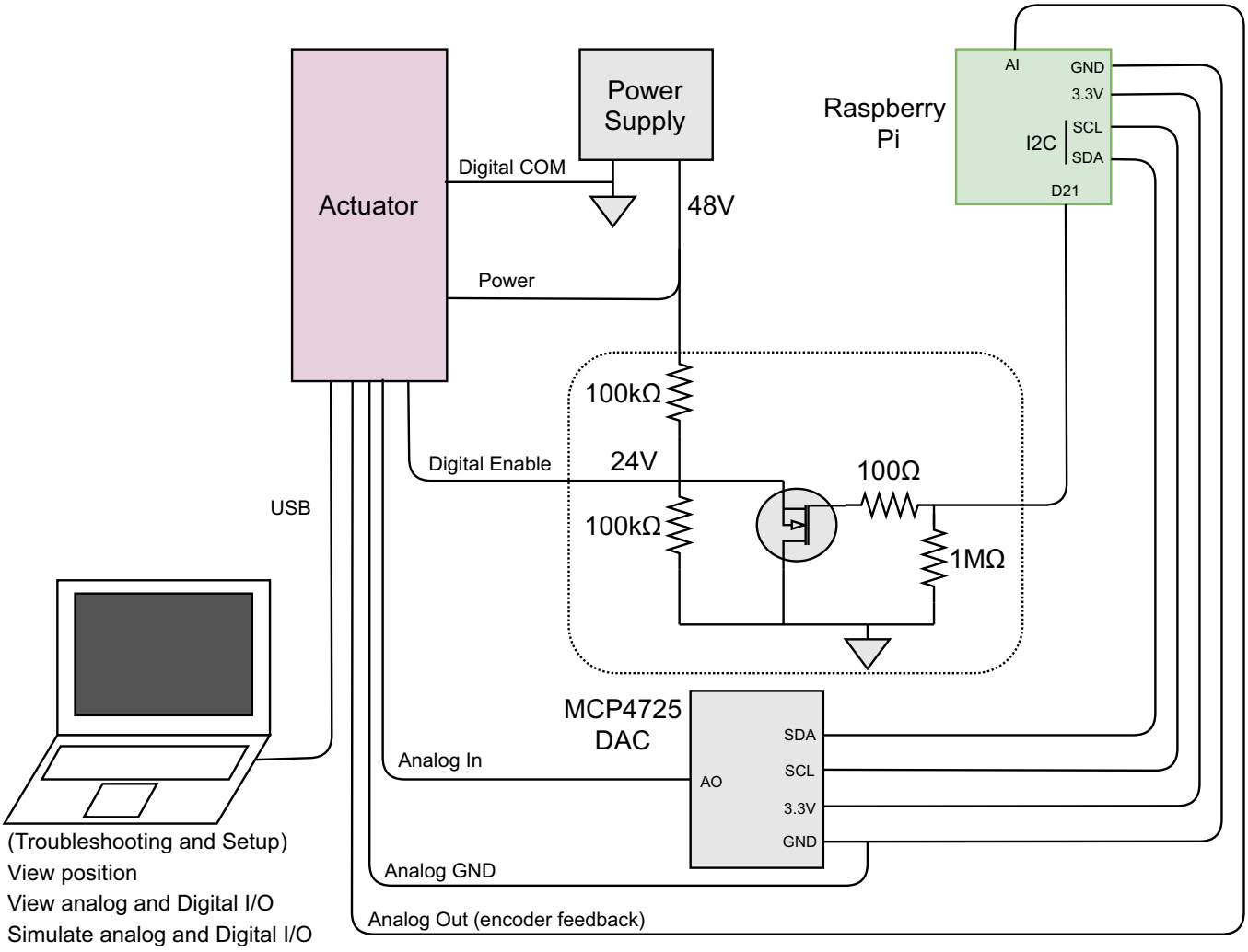

FIG. 9. Schematic of analog position control setup.

FIG. 10. Screen grabs from the breathing test. The dotted lines indicate maximum inhalation, while the dashed lines indicate maximum exhalation. The tidal volume is 892 ml. Note that the camera angle on the right and left lungs are slightly different to show a different cross-section of the trajectory. The view of both lungs show that they move almost identically.

To characterize the consistency of relative lesion position inside the lungs during motion, CT scans were performed at 0%, 50%, and 100% inhalation for three sequential breathing cycles. The phantom was then set to breathe continuously for 150 cycles, and a further series of three scans was obtained to detect any shifts in the

TABLE III. Lung trajectory comparison.

Parameter	Wade et al.[3]	Phantom	Scaled
Tidal Volume	799 ± 210 ml	892 ml	799 ml
Axial Extension	1.7 ± 0.26 cm	1.4 cm	1.3 cm
Circumference Increase	6.8 ± 2.2 cm	8.4 cm	7.5 cm

The "scaled" column is the measured parameters normalized to match Wade's tidal volume for ease of comparison (assuming the parameters scale approximately linearly with volume in this range)

lesion position (i.e. 12 scans in total). The measured *x, y, z* coordinates of lesion centroids in the left and right lung are plotted in Fig. 11(bottom). The graphs demonstrate consistent lesion trajectories between sequential breathing cycles, as well as after 150 untracked cycles. The average standard error of the mean for 0%, 50%, and 100% inhalation was 0.23, 0.24, and 0.09 mm in the anterior–posterior, transverse, and axial coordinates, respectively, for all six lesions. Overall, the lungs moved in a controllable manner and it was found that the lesions did not shift out of position during respiration. A small drift of ~2 mm was found with the posterior lesion in the left lung. The respiration kinetics were realistic, with 920 ml tidal volume and 10–20 breaths per minute tested. Further videos and CT data can be found on the open source link below.

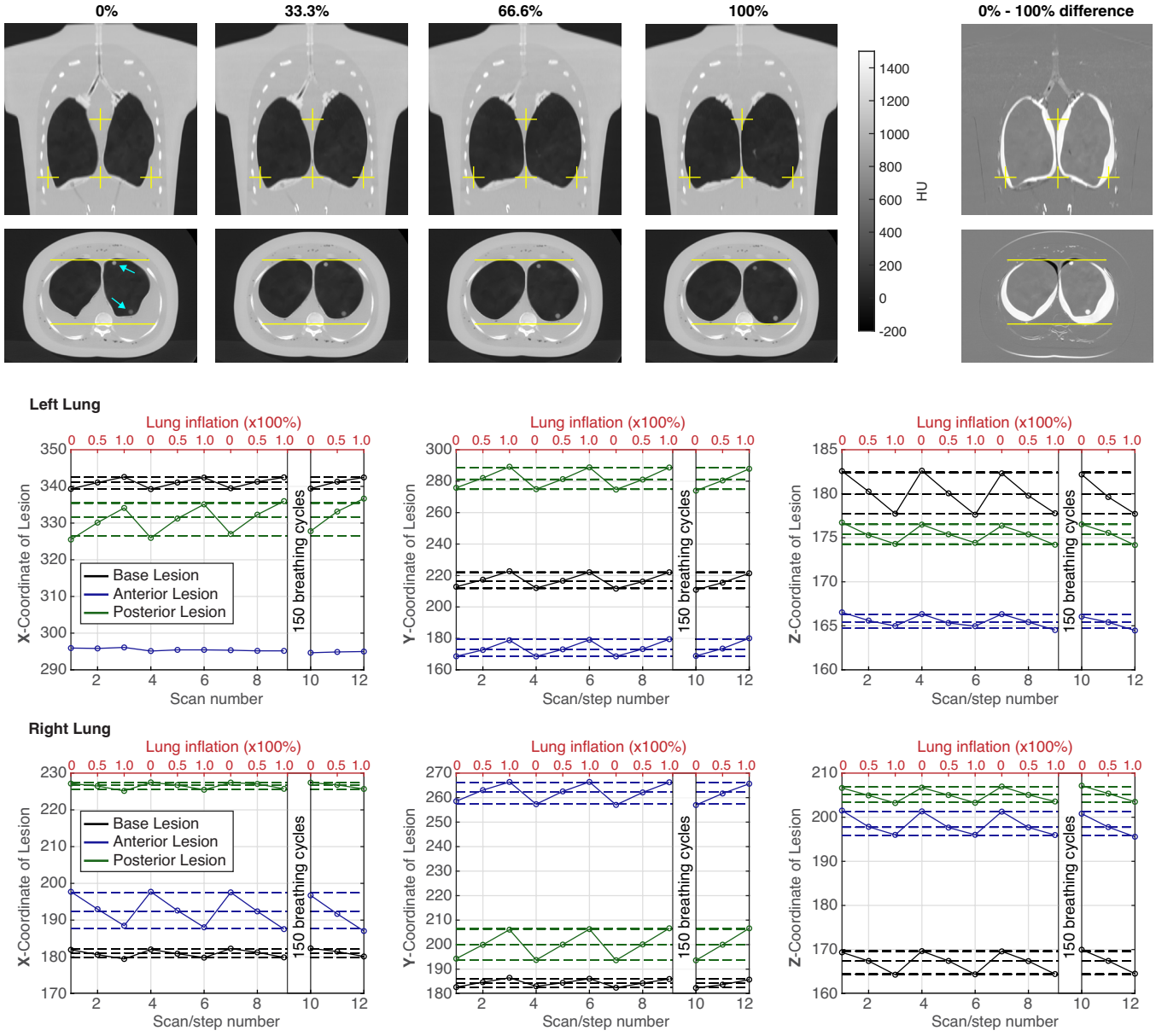

FIG. 11. (Top) Coronal and transverse planes of CT scans of the phantom corresponding to 0%, 33.3%, 66.6%, and 100% lung inflation, and the difference image between 0% and 100% inflation. Yellow markers are added for reference, and blue arrows indicate artificial lesions. (Bottom) X (anterior-posterior), Y (left-right), and Z (inferior-superior) coordinates of the three lesions in the left and right lungs, measured at 0%, 50%, and 100% inhalation for three successive breaths, followed by a fourth series of measurements after 150 cycles. All lesions show small deviations from their mean positions (dashed lines).

4. DISCUSSION

We have developed and validated the main aspects of the phantom design and usability, including materials, fabrication, couplings, actuation, dynamics, control, and procedures, such as filling the phantom. These elements have been shown to work together well to achieve the desired purpose of modeling nonrigid lung motion inside an anthropomorphic phantom. The design objectives of consistent, controllable, symmetric, and realistic motion have been met, although there are a few aspects that can be improved in future iterations.

In normal respiration, lungs typically expand more axially than cross-sectionally.[7] In the developed phantom, the lung expansion was more uniform. Thus, artificial lesions attached to inferior lobes of the manufactured lungs travel a shorter path on average compared to reality (for a similarly-sized person). Two approaches can be taken to increase the axial expansion. First, the lungs could be coupled directly to the piston using an elastic cord. Making this coupling looser or tighter would produce more or less axial extension, while also keeping the lungs centered in the antero-posterior direction. Alternatively, during the lung fabrication the wall material (Chlorosil) can be strategically rolled thinner in parts that should expand more.

In addition, though the ribs flex to accommodate the lung expansion, the torso shell is rigid, so the lungs are forced to expand dorsally instead of the chest rising as it does in humans. However, by attaching the lungs to the spine so they do not float up when the phantom is placed in a supine position, they can expand upwards during inhalation. In this way, lesions placed on the lungs near the chest retain the expected, anatomically correct trajectory, though their motion relative to the ribs may differ slightly from that in patients.

A limitation of the current design is that with foam inside the lungs, the gamma attenuation coefficient of the lungs was approximately 15% of that for soft tissue, whereas in reality, it should be around 40%.[23] This could be addressed in the future by more carefully selecting the foam material, and possibly by adding water to the foam.

Foam can also be used to fill the space outside the lungs to introduce realistic image heterogeneity through small air bubbles caught in the foam and to facilitate organ placement (liver and heart), as shown previously in the Probe-IQ.[22,23] The foam could also potentially transmit the lung motion to the other organs, leading, for example, to liver motion, and lesions can be placed in arbitrary locations by cutting pockets into the foam. Here the foam's effect on lung expansion, and the potential for all the bubbles to escape the foam under the constant motion must be assessed. To improve the realism of motion and deformation of other organs, they could also be manufactured using the same method as the lungs out of silicone elastomer.

By means of optical tracking and sequential CT scans, we found that the phantom motion was consistent between breaths. Since the actuator is very precise and can be programmed with the exact same motion, the movement is also expected to be consistent between different tests (i.e. scan repetitions). Any possible movement variations between tests would stem from changes in the initial lung axial position, rotation, and inflation. Positional changes are mitigated using foam around the ribs which ensures a similar setup every time,[23] and by marking a point on the trachea that aligns with a mark on the phantom neck port to ensure consistent alignment. A pressure gauge can be used to obtain consistent initial inflation of the lungs.

The described phantom design, materials, and principle of operation can facilitate the construction of similar phantoms elsewhere, and guide the development of a next iteration of phantoms for PET/CT imaging. For this purpose, we have documented and made available open-source every detail of the design. While the anthropomorphic shell, ribs, and organs for the Probe-IQ phantom are for the most part commercially available (Radiology Support Devices, Inc., Long Beach, CA), the focus of this work is the addition of lungs and a motion mechanism, which can be adapted to other phantoms. Indeed, the linear actuator is commercially available while the designs of all other components are available with fabrication instructions (see Open Source section).

Once COVID-19 restrictions at our center are eased, pilot PET scans will be performed to characterize the effect of lung motion on lesion quantification in a realistic environment. In future work, we will report the results of initial PET scans, compare the performance to previously created phantoms from literature, and investigate methods to further improve the realism of the lung motion.

5. CONCLUSION

In this work, we presented a method and mechanical design to incorporate anatomically accurate, elastic lungs and respiratory motion into an anthropomorphic phantom for PET/CT imaging. The proposed physical principle of operation, materials, couplings, and electronics have been validated. A new method to fabricate elastic lung models using 3D-printed molds was established and tested, and a software interface to plan and visualize these breathing patterns was developed, with two separate control schemes. The design can achieve a variety of respiratory wave-forms with up to 25 breaths per minute at 1232 ml tidal volume, and is expected to contribute to studies evaluating the effect of respiratory motion on detectability and quantification of cancer lesions.

OPEN SOURCE

To promote further development of PET/CT and phantom technology, we have open-sourced the entire design, including all CAD files, code, engineering drawings, and more, with supporting documentation. This material can be found here: https://github.com/dgblack/robotPhantom.

ACKNOWLEDGMENT

We gratefully acknowledge support by Daryl Murphy, David Moe, and Malena Rapaport at Barber Prosthetics

(Vancouver, Canada) in all aspects related to lung manufacturing. Robert de Rot at PQ Systems Ltd (Vancouver, Canada) provided guidance and a demo linear actuator for initial testing. Foam samples were provided by Discount Foam (Vancouver, Canada). This work was supported by the National Institutes of Health (NIH) / Canadian Institutes of Health Research (CIHR) Quantitative Imaging Network (QIN) Grant number 137993, and by BC Cancer Foundation. We also gratefully acknowledge the Engineering Physics Project Lab at the University of British Columbia for financial and expertise support.

CONFLICT OF INTEREST

The authors have no conflicts to disclose.

[a]Author to whom correspondence should be addressed. Electronic mail: arman.rahmim@ubc.ca

REFERENCES

1. Valk PE, Abella-Columna E, Haseman MK, et al. Whole-body PET imaging with [18F]fluorodeoxyglucose in management of recurrent colorectal cancer. *Arch Surg*. 1999;134:503–511. http://www.ncbi.nlm.nih.gov/pubmed/10323422.
2. Dawood M, Lang N, Jiang X, Schäfers KP. Lung motion correction on respiratory gated 3-D PET/CT images. *IEEE Trans Med Imaging*. 2006;25:476–485.
3. Wade OL. Movements of the thoracic cage and diaphragm in respiration. *J Physiol*. 1954;124:193–212.
4. Nayyeri F. A review on motion correction methods in PET/CT images for detection of cancer cells. *Acta Medica Bulg*. 2015;42:68–78.
5. Schmitz R, Alessio A, Kinahan P. The Physics of PET/CT Scanners.
6. Nehmeh SA, Erdi YE, Ling CC, et al. Effect of respiratory gating on reducing lung motion artifacts in PET imaging of lung cancer. *Med Phys*. 2002;29:366–371.
7. Doot RK, McDonald ES, Mankoff DA. Role of PET quantitation in the monitoring of cancer response to treatment: review of approaches and human clinical trials. *Clin Transl imaging*. 2014;2:295–303.
8. Hayden AR, Tonseth P, Lee DG, et al. Outcome of primary mediastinal large B-cell lymphoma using R-CHOP: impact of a PET-adapted approach. *Blood J Am Soc Hematol*. 2020;136:2803–2811.
9. Guerra L, De Ponti E, Elisei F, et al. Respiratory gated PET/CT in a European multicentre retrospective study: added diagnostic value in detection and characterization of lung lesions. *Eur J Nucl Med Mol Imaging*. 2012;39:1381–1390.
10. Manber R, Thielemans K, Hutton B, et al. Clinical impact of respiratory motion correction in simultaneous PET/MR, using a joint PET/MR predictive motion model. *J Nucl Med*. 2019;59:1467–1493.
11. Rakvongthai Y, El Fakhri G. Magnetic resonance-based motion correction for quantitative PET in simultaneous PET-MR imaging. *PET Clin*. 2017;12:321–327.
12. Sureshbabu W, Mawlawi O. PET/CT imaging artifacts. *J Nucl Med Technol*. 2005;33:156–161.
13. Chi A, Nguyen N. 4D PET/CT as a strategy to reduce respiratory motion artifacts in FDG-PET/CT. *Front Oncol*. 2014;4:205.
14. Geramifar P, Zafarghandi MS, Ghafarian P, Rahmim A, Ay MR. Respiratory-induced errors in tumor quantification and delineation in CT attenuation-corrected PET images: effects of tumor size, tumor location, and respiratory trace: a simulation study using the 4D XCAT phantom. *Mol Imaging Biol*. 2013;15:655–665.
15. Siman W, Mawlawi OR, Mikell JK, Mourtada F, Kappadath SC. Effects of image noise, respiratory motion, and motion compensation on 3D activity quantification in count-limited PET images. *Phys Med Biol*. 2016;62:448.
16. Cui Y, Bowsher J, Cai J, Yin F-F. Impact of moving target on measurement accuracy in 3D and 4D PET imaging—a phantom study. *Adv Radiat Oncol*. 2017;2:94–100.
17. Kawano T, Ohtake E, Inoue T. Deep-inspiration breath-hold PET/CT of lung cancer: maximum standardized uptake value analysis of 108 patients. *J Nucl Med*. 2008;49:1223–1231.
18. Liu C, Pierce LA II, Alessio AM, Kinahan PE. The impact of respiratory motion on tumor quantification and delineation in static PET/CT imaging. *Phys Med Biol*. 2009;54:7345.
19. Walker MD, Bradley KM, McGowan DR. Evaluation of principal component analysis-based data-driven respiratory gating for positron emission tomography. *Br J Radiol*. 2018;91:20170793.
20. Zhang X, Xie Z, Berg E, et al. Total-body dynamic reconstruction and parametric imaging on the uEXPLORER. *J Nucl Med*. 2020;61:285–291.
21. Gillies RJ, Kinahan PE, Hricak H. Radiomics: images are more than pictures, they are data. *Radiology*. 2016;278:563–577.
22. Kadrmas D, Casey M, Conti M, Jakoby B, Lois C, Townsend D. Impact of time-of-flight on PET tumor detection. *J Nucl Med*. 2009;50:1315–23.
23. Kadrmas D, Casey M, Black N, Hamill J, Panin V, Conti M. Experimental comparison of lesion detectability for four fully-3D PET reconstruction schemes. *IEEE Trans Med Imaging*. 2009;28:523–34.
24. Bolwin K, Czekalla B, Frohwein L, Büther F, Schäfers K. Anthropomorphic thorax phantom for cardio-respiratory motion simulation in tomographic imaging. *Phys Med Biol*. 2018;63:035009.
25. Chrysanthou-Baustert I, Polycarpou I, Demetriadou O, et al. Characterization of attenuation and respiratory motion artifacts and their influence on SPECT MP image evaluation using a dynamic phantom assembly with variable cardiac defects. *J Nucl Cardiol*. 2017;24:698–707.
26. Steidl P, Richter D, Schuy C, et al. A breathing thorax phantom with independently programmable 6D tumour motion for dosimetric measurements in radiation therapy. *Phys Med Biol*. 2012;57:2235–2250.
27. Kostiukhina N, Georg D, Rollet S, et al. Advanced Radiation DOSimetry phantom (ARDOS): a versatile breathing phantom for 4D radiation therapy and medical imaging. *Phys Med Biol*. 2017;62:8136–8153.
28. Perrin RL, Zakova M, Peroni M, et al. An anthropomorphic breathing phantom of the thorax for testing new motion mitigation techniques for pencil beam scanning proton therapy. *Phys Med Biol*. 2017;62:2486–2504.
29. Perrin R, Peroni M, Bernatowicz K, et al. SU-D-BRE-01: a realistic breathing phantom of the thorax for testing new motion mitigation techniques with scanning proton therapy. *Med Phys*. 2014;41:111.
30. Colvill E, Krieger M, Bosshard P, et al. Anthropomorphic phantom for deformable lung and liver CT and MR imaging for radiotherapy. *Phys Med Biol*. 2020;65:07NT02.
31. Hubbell JH, Seltzer SM. X-Ray Mass Attenuation Coefficients. Radiation Physics Division, Physics Measurement Laboratory, National Institute of Standards and Technology. 2004. https://doi.org/10.18434/T4D01F.
32. Lindh WQ, Pooler M, Tamparo CD, Dahl BM. *Delmar's Comprehensive Medical Assisting: Administrative and Clinical Competencies*. Boston: Cengage Learning; 2009. https://books.google.ca/books?id=AUhJKmKJ_eEC.
33. Bhatt DV, Mistry KN. Experimental study of friction under different variables on a piston-cylinder assembly. http://nacomm03.ammindia.org/Articles/Dyn009.pdf
34. Merrit D, Weinhaus F. The pressure curve for a rubber balloon. *Am J Phys*. 1978;46:976–977.
35. Larson K. Can you estimate modulus from durometer hardness for silicones? Published online 2019; https://www.dow.com/content/dam/dcc/documents/en-us/tech-art/11/11-37/11-3716-01-durometer-hardness-for-silicones.pdf?iframe=true.
36. Tolomatic. ERD Electric Cylinder Features and Options. https://www.tolomatic.com/products/product-details/erd-low-cost-electric-cylinders-for-pneumatic-cylinder-replacement/features-options.